

INTERACTION OF LASER RADIATION WITH MATTER. LASER PLASMA

PACS numbers: 52.50.Jm; 52.38.Mf
DOI: 10.1070/QE2003v033n12ABEH002555

Change in the ionisation state of a near-surface laser-produced aluminium plasma in double-pulse ablation modes

V.S. Burakov, A.F. Bokhonov, M.I. Nedel'ko, N.V. Tarasenko

***Abstract*. The near-surface plasma produced upon irradiation of an aluminium target by two successive laser pulses with nonresonance and resonance wavelengths is studied by the spectroscopic and probe-assisted methods. The feasibility of increasing the ion fraction in the laser-produced plasma in double-pulse ablation modes is demonstrated. The conditions are determined under which processes on the surface as well as selective excitation and ionisation in the plasma have a determining effect on the formation of its ionisation state.**

Keywords: *laser plasma, double-pulse ablation, emission spectroscopy, resonance photoionisation.*

1. Introduction

A pulsed laser-ablated plasma produced at solid-state targets under intense laser irradiation finds applications as the atomiser of materials in laser spectral analysis [1], in the deposition of thin films of different materials [2 – 4], and in several other technological processes. Of major importance for these applications is the comprehensive understanding of the most significant physical processes that define the spatio-temporal characteristics of the near-surface plasma and the development, on this basis, of the methods for controlling the composition and energy spectrum of laser ablation products. Purposeful variation in the component and charge-state compositions of laser ablation stream is possible, in particular, by way of additional laser irradiation of the plasma.

A controllable increase in the density of excited and charged plasma particles and the variation of their energy distributions is made possible by employing double-pulse laser ablation schemes. In particular, recent publications [5, 6] show that CO_2-laser irradiation of the plasma produced at the surface of a solid target can be used to control ion energies. The IR laser radiation heats free electrons in the plasma during inverse bremsstrahlung and accelerates ions to high kinetic energies [7]. The high-energy electron collisions with neutral atoms result in their ionisation, increasing thereby the ion fraction in the plasma.

V.S. Burakov, A.F. Bokhonov, M.I. Nedel'ko, N.V. Tarasenko Institute of Molecular and Atomic Physics, National Academy of Sciences of Belarus, prosp. F. Skoriny 70, 220072 Minsk, Belarus

Received 16 August 2002; revision received 22 May 2003
Kvantovaya Elektronika **33** (12) 1065 – 1071 (2003)
Translated by E.N. Ragozin

The increase in relative ion content in a laser plasma can also be obtained by employing double-pulse ablation schemes, when the radiation of the additional laser pulse is resonantly absorbed in the plasma [3]. Our work is devoted to the study of variation in ablation plasma characteristics upon double-pulse two-frequency laser ablation.

The primary goal of our work was to find the conditions that optimise the effect exerted by additional laser radiation at the resonance frequency on the formation of component and charge-state composition of the laser plasma. We compared the ionic line intensities and time-of-flight probe characteristics in double- and single-pulse modes of plasma production. The principal mechanisms of the interaction of UV and visible laser radiation with laser-ablated aluminium plasma were analysed. Laser-induced excitation and ionisation were investigated when the target or the plasma generated at the near-surface of an aluminium target were irradiated by the 532-nm second harmonic pulses of a Nd^{3+} : YAG laser or 308-nm pulses of an excimer XeCl laser. The frequency of excimer laser radiation coincides with the resonance transition frequency of aluminium atoms.

2. Experimental

Experiments were performed using a setup shown schematically in Fig. 1. Plasma was produced by focusing the radiation of the second harmonic of a Nd^{3+} : YAG laser (10 ns, 1 – 4 J cm^{-2}) and/or an excimer XeCl laser (10 ns, 1 – 2 J cm^{-2}) on the surface of an aluminium target placed in a chamber with an atmosphere of air at a normal pressure or at a pressure of 10^{-3} Torr. Both laser radiation beams were brought into coincidence on the target surface.

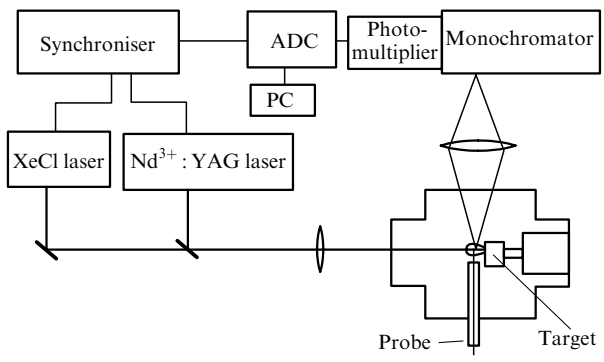

Figure 1. Scheme of the experimental setup.

The synchronisation system ensured the variation of the time delay between the laser pulses with a minimal increment of 100 ns. In experiments with additional irradiation of the plasma (not of the target), the laser ablation plasma generated by the first pulse was back-illuminated with a controllable delay by the focused radiation of the second laser near the target surface without touching it.

The emission plasma spectra were recorded with a DFS-452 spectrograph. Time-resolved measurements of the emission kinetics of individual spectral lines were performed by imaging the plasma plume onto the slit of an MDR-23 monochromator with the instrument function width of 0.05 nm. After the monochromator, the radiation was detected with an FEU-84 photomultiplier. The photomultiplier signal was recorded with a digital S9-8 oscilloscope coupled to a personal computer (PC). The oscilloscopic sweep was triggered by the leading edge of the first laser pulse.

The quantitative information on the plasma parameters, such as the electron temperature and density as well as the spatial and time evolution of atoms and ions, was partly obtained in earlier works [8 – 10] by combining the methods of time-resolved optical emission spectroscopy, laser-induced fluorescence, and time-resolved probe measurements. The concentration of aluminium atoms in the ground state was determined by exciting them with laser radiation at 394.4 nm (the $3\,^2P_{1/2} - 4\,^2S_{1/2}$ transition) and recording the fluorescence at the 396.15 nm line of Al I (the $4\,^2S_{1/2} - 3\,^2P_{3/2}$ transition).

Charged plasma particles were detected with an electric probe made of an 8-mm long molybdenum wire with diameter of 0.13 mm. The probe was placed in the chamber at a distance of 15 mm from the target surface. The probe operated into a 75-Ω load resistor. The time-of-flight characteristics of the probe current for ions and electrons were recorded when the probe voltage changed its sign.

3. Results and discussion

As shown in several papers [10 – 12], the wavelength of laser irradiation pulse plays a significant part in the formation of erosion plasma plume both at the stage of interaction of the radiation with the target surface and at the stage of its absorption in the plasma being produced. Resonance interaction effects, when laser radiation frequencies coincide with intense absorption lines, can significantly lower the plasma production threshold and raise the ion density.

To determine the effect of the laser radiation wavelength on the characteristics of erosion plasma, we first compared the integrated spectral characteristics of the plasma plumes produced by laser radiation at 535, 266, and 308 nm. In this case, for the two last wavelengths there occurred resonant absorption in the aluminium vapour. The focal spot dimensions on the target were the same in all three cases (0.7 mm × 0.6 mm), while the energies of irradiation pulses were selected so that the plasma plume emission intensities at the 358-nm line of Al II were equal. The energy densities of radiation at 532, 308, and 266 nm were 3.3, 1.6, and 2 J cm^{-2}, respectively.

A typical emission spectrum of the laser-ablated plasma produced by exposing aluminium to radiation at 532, 308, and 266 nm in air is shown in Fig. 2. It belongs to the plasma region at a distance of 0.2 mm from the target surface. The spectrum consists of lines corresponding to neutral and singly ionised excited atoms. The most intense emission lines in the visible range are the Al I (396.15 and 394.4 nm) and Al II (358.69, 466.3, 624.3, and 559.3 nm) lines. However, the intensity ratios between atomic and ionic lines and the continuous background are different for different irradiation wavelengths.

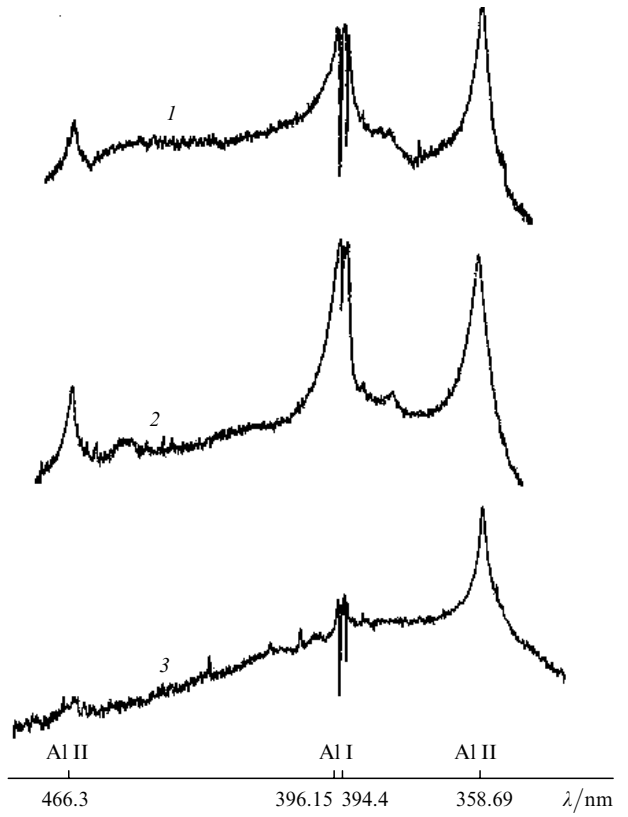

Figure 2. Emission spectrum of the laser ablation plasma produced by exposing aluminium in air to the radiation at 532 (*1*), 308 (*2*), and 266 nm (*3*).

Note that the background level in the short-wavelength part of the spectrum is high and the intensity of the 466.3-nm ionic line of Al II is strongly reduced upon ablation by the fourth harmonic of a Nd^{3+} : YAG laser. In this case, the self-reversal of the 396.15-nm and 394.4-nm atomic lines of Al I occurs, the emission in the wings being weak, which testifies to a stronger temperature nonuniformity across the cross section of the plasma plume. The most distinct line spectrum with the weakest self-reversal of the resonance lines and a significantly smaller relative contribution of a continuous spectrum is observed for excimer laser-induced ablation. The difference in the spectra is indicative of the difference in excitation and relaxation of excited states in the plasma produced by the excimer laser radiation and the harmonics of a Nd^{3+} : YAG laser.

In the case of combined action of the second harmonic pulse of a Nd^{3+} : YAG laser and the excimer laser (not shown in Fig. 2), we observed a higher degree of atomisation and higher spectral line intensities in the plasma for a double-pulse mode compared to the single-pulse mode. When the target was irradiated by two sequential laser pulses separated in time by 1, 3, 5, and 7 μs (the XeCl-laser pulse followed the second-harmonic pulse of the

Nd^{3+} : YAG laser), the 358.69-nm ionic line of Al II became narrower and the self-reversal of atomic lines was weaker.

To study the prepulse effect in greater detail, we measured the emission dynamics of the ionic (Al II, $\lambda = 358.69$ nm) and atomic (Al I, $\lambda = 396.15$ nm) lines for different time delays between the laser pulses at 532 and 308 nm. Time-resolved intensity measurements were made by recording the plasma emission from the region located at a distance of 1 mm from the target surface. The background radiation was taken into account by subtracting the signals obtained at 370 and 400 nm for the ionic and atomic lines, respectively.

The most probable processes responsible for the population of levels are electron collisions with neutral atoms and electron – ion recombination [13].

The relative intensities $J = (I^{d}_{max} - I^{d}_{ph})/(I^{s}_{max} - I^{s}_{ph})$ [where $I^{d,s}_{max}$ and $I^{d,s}_{ph}$ are the peak and background intensities in the double- (d) and single-pulse (s) modes] for the 358.69-nm Al II ionic line as functions of the time delay Δt between the pulses are given in Fig. 3a. The largest increase in the relative intensity takes place for delays $\Delta t = 3 - 5$ μs; in this case, J is hardly dependent on the sequence order of the laser irradiation pulses with different wavelengths. For $\Delta t > 7$ μs, J was observed to fall off. A higher relative intensity is attained when the XeCl-laser pulse comes second. This may be related to the resonance nature of the exciting radiation with $\lambda = 308$ nm, which is responsible for the excitation and ionisation of aluminium atoms. However, the main contribution to the increase of emission (of ion density) is supposedly made by processes at the surface, in particular the increase in material ablation from the surface preirradiated by the pulse of the first laser. It is noteworthy that focusing the XeCl-laser radiation in the plasma (and not on the target surface) resulted in the emergence of a signal at the 358.69-nm ionic line of Al II in the 0 – 2 μs range of time delays [curve (*3*) in Fig. 3b]. In this time interval, plasma processes make a certain contribution to the observed increase in ionic line intensity. However, the effect of plasma decays rapidly with increasing time delay, when the laser radiation is relatively weakly absorbed in the plasma owing to its expansion and goes primarily into ablation.

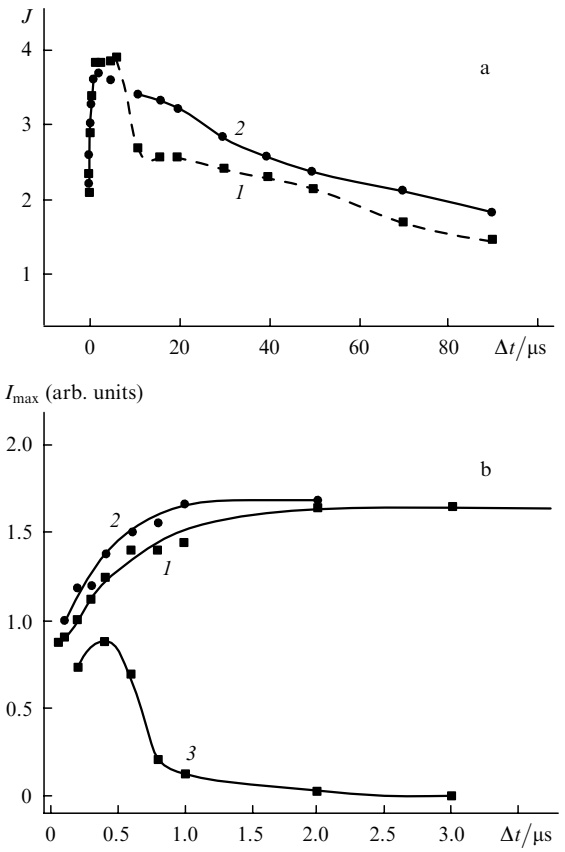

Figure 3. Relative intensity J (a) and peak signal intensity I_{max} (b) for the 358.69-nm ionic Al II line in the double-pulse mode as functions of the time delay Δt between the pulses under sequential target irradiation by the pulses of excimer laser radiation and the second harmonic of the Nd^{3+} : YAG laser (*1*), in the case of their reverse order (*2*), and with XeCl-laser focusing into the plasma produced by the second harmonic pulse of Nd^{3+} : YAG laser radiation (*3*). The measurements were performed in air at a normal pressure.

The above data (Fig. 3) were obtained upon the laser ablation of aluminium in the air atmosphere at a normal pressure. Similar measurements when the chamber was evacuated to 10^{-3} Torr are given in Fig. 4. In this case, the increase in the peak intensity of the ionic line for a sequential double-pulse irradiation (the prepulse effect) rapidly decays in the 0 – 0.5 μs interval owing to a higher plasma expansion velocity. Like in the case of normal pressure, the effect is stronger when the excimer laser acts second. The expansion velocity of the plasma plume was estimated from the slope of the curve which shows the delay of the peak of ion emission intensity as a function of the distance to the target. It was equal to about 1.2×10^{6} cm s^{-1} for a laser radiation energy density of 2.5 J cm^{-2}.

The prepulse effect for atomic lines is weaker, which is in agreement with experimental observations of other authors [14 – 16]. The time-resolved emission intensity of the 396.15-nm atomic line of Al I from laser ablation plasma under single- and double-pulse irradiation is shown in Fig. 5. The

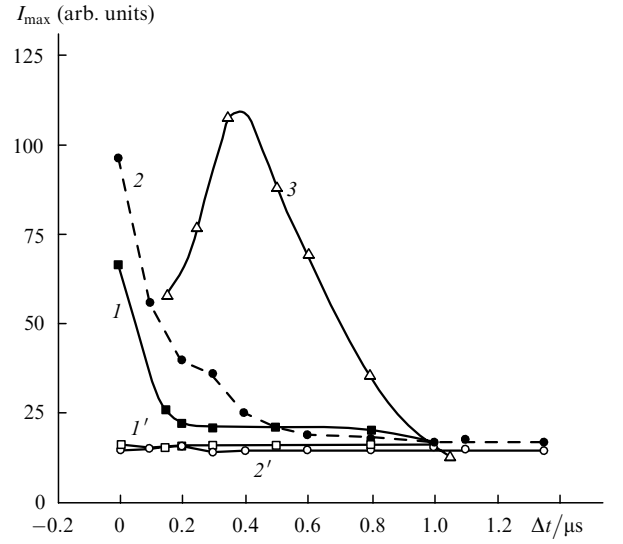

Figure 4. Intensities of the 358.15-nm ionic line of Al II at the peak of the signal I_{max} as functions of the time delay Δt between the pulses under sequential irradiation in vacuum at 308 and 532 nm (*1*) and 532 and 308 nm (*2*), average values of the corresponding signals in the absence of a prepulse (*1′*, *2′*), and time dependence of the amplitude of the fluorescence signal of aluminium atoms at the 396.15-nm line of Al I (*3*).

observed sharp peak 1 results from the resonance interaction of XeCl-laser radiation with aluminium atoms in the ground state produced after the target irradiation by the first laser pulse. The small second emission peak 2 arises from excited atoms produced in the near-surface ablation by the XeCl-laser pulse. For moderate delays ($0 \leqslant \Delta t \leqslant 1$ μs), the aluminium plasma with ground-state atoms produced by the first pulse attenuates the XeCl-laser radiation. That is why the 396.15-nm line of Al I is not stronger in the double-pulse ablation (peak 2) than in the single-pulse irradiation mode (peak 3). At the same time, the time of radiation of the above atomic line lengthens in the presence of a prepulse. Curve (*3*) in Fig. 4 serves to illustrate the time range in which ground-state atoms exist in the observation region.

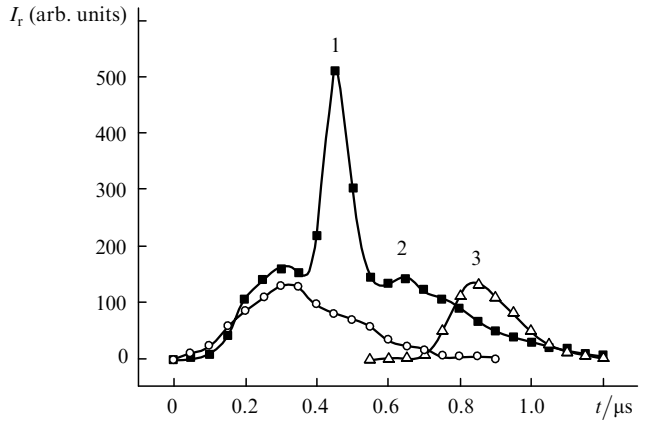

Figure 5. Oscilloscope traces of laser-plasma radiation pulses at the 396.15-nm line of Al I in the double-pulse aluminium ablation by the sequence of the 532-nm and 308-nm pulses (■) and single-pulse laser ablation by these pulses [532 (○) and 308 nm (△)]; 1–3 are numbers of emission peaks.

The time-of-flight characteristics of charged plasma particles were investigated by the probe technique. The aim was to find out whether the observed rise in ionic line intensities in the double-pulse regime resulted from a change in their excitation conditions or was related to the fact that the ion plasma density increased in the case of target ablation by the sequence of two pulses.

We determined preliminary the change in the ion density for different energy densities of laser radiation Φ in the single-pulse mode. The threshold energy density of laser radiation which ensures the detectable number of ions, is 0.3 J cm^{-2} at 1064 nm and 0.05 J cm^{-2} at 308 nm. Above the threshold, with increasing Φ up to 5 J cm^{-2} we observed a rise in ion density; the ion signal did not reach saturation as opposed to the fluorescence signal, which exhibited saturation with increasing Φ. The build-up in ion density can be attributed to the increase in the amount of material removed from the target surface and the fraction of laser energy absorbed in ablation products, which is responsible for heating and subsequent collisional ionisation. The resultant data showed that for laser radiation energy densities $\Phi > 1$ J cm^{-2} the degree of ionisation of the plasma in the initial stage is rather high but lowers rapidly in the first few hundreds of nanoseconds.

When two sequential laser pulses were used for ablation, the probe time-of-flight curves (both for ions and electrons) for the plasma of the second laser pulse with a prepulse (double-pulse laser ablation) were found to differ significantly from the probe curves in the absence of a prepulse (single-pulse laser ablation). A typical signal of electron probe cur-rent is shown in Fig. 6. The time dependence of the electron probe current has several (up to three) peaks, which are located close to the peaks of the time dependence of the ion current. Initially, the electron current probe curve shows a short pulse caused by the photoelectrons emitted from the target surface prior to the intensive evaporation. These photoelectrons are not electrostatically coupled to ions and therefore travel with a high velocity towards the probe. One can see from Fig. 6 that the additional laser pulse irradiating the target is responsible for a sharp increase of the density of charged particles in the plasma. This increase was observed in a wide range of time delay between the pulses, this increase being larger when the second pulse in the double-pulse ablation was the radiation pulse of an excimer laser.

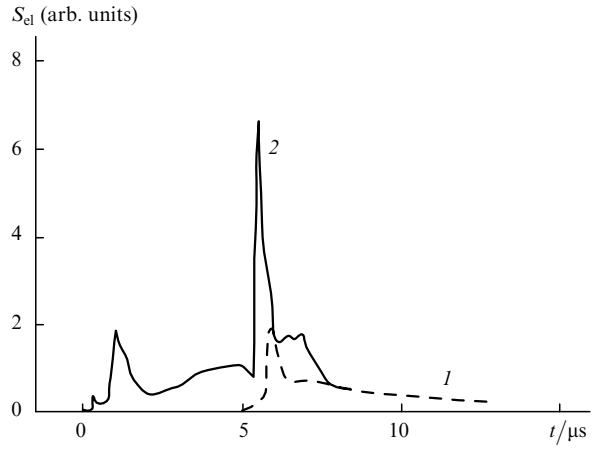

Figure 6. Shape of electron current probe pulses (for a probe potential of −27 V) without (*1*) and with (*2*) the second harmonic Nd^{3+}:YAG-laser prepulse.

To explain these dependences, we analyse the possible mechanisms of laser radiation absorption in the plasma produced by the first pulse and of increasing its degree of ionisation. When the target is irradiated by nanosecond pulses, the material evaporation begins when the pulse front reaches the target surface. The production of a near-surface plasma is commonly related [17, 18] to the processes of interaction between the remaining part of the laser pulse and ablation products: the heating and avalanche-like ionisation of the vapour. The mechanisms of plasma production in the context of double-pulse laser ablation have not been adequately studied. Until the present time, the sequential irradiation of a solid surface by two laser pulses was primarily employed in the spectral analysis to raise the intensities of analytic lines [14–16]. There are only a few papers concerned with the study of the variation in plasma parameters under irradiation by additional laser pulses [19, 20].

The features of plasma production with a prepulse will be considered by analysing the interaction of the additional laser pulse with the surface and the near-surface plasma produced by the first pulse. It is noteworthy that the conditions of this interaction vary with lengthening the

time interval between the pulses as a result of the variation in the plasma density and composition in the course of expansion and cooling as well as a result of the change in optical and thermal surface properties. To interpret the resultant data we will proceed from the frequency dependence of the efficiency of laser radiation absorption by the target surface and the near-surface plasma.

The two principal mechanisms of radiation absorption in a laser-produced plasma at moderate intensities are inverse bremsstrahlung and photoionisation. The absorption coefficient due to inverse bremsstrahlung is proportional to the cube of the radiation wavelength [21]. This dependence has the effect that the absorption coefficient for the second harmonic (532 nm) of Nd^{3+} : YAG-laser radiation is almost five times greater than the absorption coefficient for the radiation of an excimer XeCl laser. In the UV spectral range, however, direct photoionisation can play a significant part, since the photon energy becomes comparable with the ionisation energy of excited atoms. Note also that the photoionisation-induced rise in electron and ion densities, can substantially increase the photon absorption probability due to the inverse bremsstrahlung in electron – ion collisions. The results of experimental investigations [22] have confirmed the efficiency of photoionisation mechanism in the UV laser ablation of metal targets. Of particular interest are the cases of resonance interaction, when the frequencies of laser radiation coincide with intense absorption lines. A sharp rise of the absorption cross section in the resonance wave field [23] may substantially increase the electron energy build-up rate, resulting in the complete ionisation of metal atoms in the resonance radiation field in a time of the order of the energy build-up time.

Analysing the above processes for the aluminium plasma we note that the first excited level of aluminium atoms is located 3.14 eV higher than the ground state, while the ionisation potential of aluminium is 5.99 eV. That is why the photoionisation via intermediate levels is possible for the fourth harmonic (266 nm) of Nd^{3+} : YAG-laser radiation and the XeCl-laser radiation (308 nm), while two-photon ionisation is required for the radiation in the visible range (2.31 eV for $\lambda = 532$ nm).

The calculated data on the time evolution of absorption coefficient of aluminium plasma are given in Table 1 and Fig. 7. The absorption coefficient α was estimated from the expression [11, 12]

$$\alpha = \alpha_{ib} + \alpha_{phi} \approx 1.27 \times 10^{-46} Z^2 \lambda^3 T_e^{-0.5} n_i \times \left[1 - \exp\left(-\frac{hv}{T_e}\right)\right] n_e + \sum_m 2.9 \times 10^{-17} \frac{(I - \varepsilon_m^*)^{2.5}}{(hv)^3} n_m, \quad (1)$$

where n_i and n_e are the ion and electron densities (in cm^{-3}); λ is the wavelength of laser radiation (in nm); T_e is the electron temperature (in eV); hv is the photon energy (in eV); Z is the ionic charge; and I is the ionisation potential. The first term (α_{ib}) in formula (1) is due to inverse bremsstrahlung and the second one (α_{phi}) is related to the photoionisation of atoms excited to a state with an energy $\varepsilon_m^* > I - hv$. Their density is $n_m = n_0(g_m/g_0)\exp(-\varepsilon_m^*/T_e)$, where g_m and g_0 are the statistical weights of the mth and zero levels; and n_0 is the population density of the ground level. For the excimer laser, account was taken of the $3d\,^2D_{3/2}$ excited-level population growth arising from resonance radiation absorption, with $n_m = n_0 g_m/(g_m + g_0)$ in saturation. The $3p\,^2P^0_{1/2} - 3d\,^2D_{3/2}$ transition frequency of aluminium atoms (308.21 nm) falls into the lasing range of the XeCl laser, and therefore exposure to the radiation of this laser leads to the excitation of atoms from the $3p\,^2P^0_{1/2}$ ground level to the $3d\,^2D_{3/2}$ level with their subsequent ionisation.

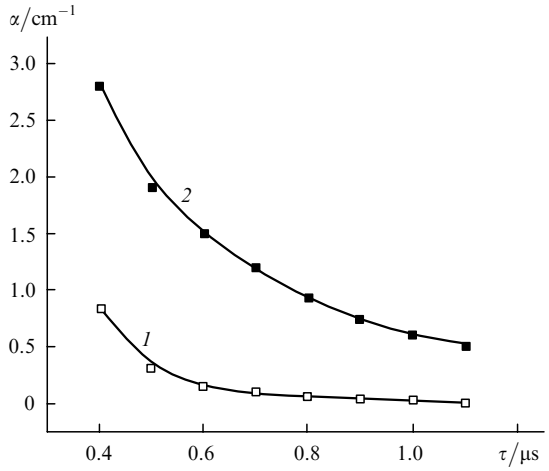

Figure 7. Time dependences of the absorption coefficient of the aluminium plasma calculated at 532 (*1*) and 308 nm (*2*).

In the calculation by formula (1), advantage was taken of the experimentally measured time dependences of electron and atomic densities of the decaying aluminium plasma. In this case, the electron density was determined from the measured widths of emission lines in accordance with the theory of Stark broadening. The profiles of individual selected lines were analysed for different delays to obtain the temporal evolution of n_e. The electron temperature was determined from the Boltzmann method. The methods and the results of determination of the electron

Table 1.

$\tau/\mu s$	$n_e/10^{18}$ cm^{-3}	$n_a/10^{17}$ cm^{-3}	T_e/eV	$\alpha_{ib}/10^{-3}$ cm^{-1}		α_{phi}/cm^{-1}	
				$\lambda = 532$ nm	$\lambda = 308$ nm	$\lambda = 532$ nm	$\lambda = 308$ nm
0.4	0.83	5.3	1.35	9.3	2.1	0.85	2.8
0.5	0.56	3.8	1.1	5	1.08	0.31	1.9
0.7	0.24	2.4	0.93	1	0.22	0.1	1.2
0.9	0.24	1.5	0.88	0.98	0.2	0.05	0.74
1.1	0.15	1.07	0.88	0.45	0.09	0.02	0.53

Note: n_a is the atomic number density.

density and temperature in the laser-produced plasma were described in greater detail in our previous paper [9]. The measurement data on the plasma parameters (n_e, T_e, n_a) at different points in time τ after target irradiation by the laser pulse are given in Table 1.

One can see from Fig. 7 that the time delay range in which the radiation absorption in the plasma of the first laser pulse is significant does not exceed 1 μs, which is in agreement with experimental data (Fig. 3b). Note that the mechanism of two-step resonance ionisation via an intermediate level continues to operate for the excimer-laser radiation even after the decay of the plasma of the first pulse because of the longer lifetime of the vapour-and-gas cloud near the target surface. In this case, the rate of charged-particle production is defined by the density of atoms in the ground state and the rate coefficients for ionisation involving resonantly excited atoms. According to Ref. [24], the cross section σ_{pi} for the ionisation of aluminium atoms from the $3d\ ^2D_{3/2}$ excited level by the excimer XeCl-laser radiation is equal to $(5.6 \pm 1.1) \times 10^{-18}$ cm^2, while the value calculated in Ref. [24] is 2.4×10^{-18} cm^2. The rate of excited-atom photoionisation under irradiation with a power density $P = 5 \times 10^8$ W cm^{-2}, defined by expression the $W = \sigma_{pi} P/hv$, amounts to 4.3×10^9 s^{-1} for a radiative decay probability of the $3d\ ^2D_{3/2}$ level equal to 1.37×10^8 s^{-1}. The energy density of laser radiation in the photoionisation channel corresponding to the ionisation of each atom that experiences excitation is estimated at $\sim$0.14 J cm^{-2}.

Based on the research performed and an analysis of the literature [14–17], we can assume that the following picture of temporal plasma evolution takes place in the cases of single- and double-pulse ablation. After the front of a single laser pulse evaporates the target material and produces the plasma (by way of inverse bremsstrahlung in the initial vapour-and-gas cloud), the screening conditions are fulfilled for relatively high radiation intensities and the near-surface ablation terminates. At the same time, an intense material evaporation is responsible for a sharp increase in the pressure initiating a shock wave in the surrounding atmosphere, with the result that the remaining part of the laser pulse is absorbed at the shock front. In general, three main regions may be distinguished in the laser ablation in the atmosphere: the target surface, the erosion plasma containing the main part of vaporised material, and the plasma shell (the shock front) [16]. In the case of a single pulse, a significant part of the pulse may be screened by the shock front and not penetrate into the plasma core region.

The situation is different when the target surface is irradiated by two pulses with some delay between them. After the first pulse, the plasma expands and recombines, and the electron density decays rapidly with time. The second pulse travels through a relatively tenuous plasma and is therefore capable of penetrating it, more efficiently exciting the ablation products and interacting with the near-surface. This results in an increase of the amount of vaporised material as well as of its degree of excitation and ionisation.

4. Conclusions

Therefore, our spectroscopic and probe-assisted measurements of the plasma produced near the surface of an aluminium target irradiated by two sequential laser pulses have demonstrated the feasibility of increasing the degree of plasma ionisation. We have determined the time interval that maximises the relative intensities of ionic lines, which amount to five for the parameters of laser pulses used in our experiments.

The observed rise in plasma emission may be due to the efficiency increase in the interaction between the second laser pulse and the target surface, resulting in the increase in the amount of vaporised material and the improvement of its excitation conditions in the presence of the plasma of the first pulse. The efficiency of excited-particle production rises because of selective laser excitation due to the resonance interaction between the second pulse and the plasma.

The interaction between the second laser radiation and the near-surface plasma produced by the first laser pulse, which is affected by way of inverse bremsstrahlung and photoionisation absorption, is significant only for short time delays (0 – 1.5 μs after the first laser pulse). The results of spectroscopic measurements are confirmed by the analysis of probe measurements, which revealed an increase in density of charged particles in the plasma produced in the double-pulse ablation. The increase in the degree of ionisation of the laser ablation plasma with the proper choice of wavelengths and the time interval in the pulse sequence can be employed to optimise several technological processes and to improve laser spectral analysis.

Acknowledgements. This work was supported in part by the Belorussian Foundation for Basic Research (Grant No. 03-177).

References

1. *OSA Trends in Optics and Photonics (TOPS). Vol. 81. Laser Induced Plasma Spectroscopy and Applications* (Washington DC, Optical Society of America, 2002).
2. Chrisey D.B., Hubler G.K. (Eds) *Pulsed Laser Deposition of Thin Films* (New York: Wiley, 1994).
3. Cuomo J., Pappas D.L., Bruley J., Doyle J.P., Saenger K.L. *J. Appl. Phys.*, **70**, 1706 (1991).
4. Novodvorskii O.A., Filippova E.O., Khramova O.D., Shevelev A.K., Wenzel C., Bartha J.W. *Kvantovaya Elektron.*, **31**, 159 (2001) [*Quantum Electron.*, **31**, 159 (2001)].
5. Dem'yanenko A.V., Letokhov V.S., Puretskii A.A., Ryabov E.A. *Kvantovaya Elektron.*, **25**, 36 (1998) [*Quantum Electron.*, **28**, 33 (1998)].
6. Mukherjee P., Cuff J.B., Witanachi S. *Appl. Surf. Sci.*, **127–129**, 620 (1998).
7. Wheeler C.B., Fielding S.J. *Plasma Phys.*, **12**, 551 (1970).
8. Burakov V.S., Bokhonov A.F., Nedel'ko M.I., Tarasenko N.V., in *Progress in Plasma Processing of Materials* (Amsterdam: Elsevier, 2001) p. 661.
9. Burakov V.S., Bokhonov A.F., Naumenkov P.A., Nedel'ko M.I., Tarasenko N.V. *Zh. Prikl. Spektrosk.*, **65**, 426 (1998).
10. Burakov V.S., Bokhonov A.F., Nedel'ko M.I., Tarasenko N.V. *Appl. Surf. Sci.*, **138–139**, 350 (1999).
11. Amoruso S., Armenante M., Berardi V., Bruzzese R., Spinelli N. *Appl. Phys. A*, **65**, 265 (1997).
12. Gaidarenko D.V., Leonov A.G. *Pis'ma Zh. Tekhn. Fiz.*, **18**, 21 (1992).
13. Knudtson J.T., Green W.B., Sutton D.G. *J. Appl. Phys.*, **61**, 4771 (1987).
14. Petukh M.L., Rozantsev V.A., Shirokanov A.D., Yankovskii A.A. *Zh. Prikl. Spektrosk.*, **67**, 798 (2000).
15. Pershin S.M. *Kvantovaya Elektron.*, **16**, 325 (1989) [*Sov. J. Quantum Electron.*, **19**, 215 (1989)].
16. St-Onge L., Detalle V., Sabsabi M. *Spectrochim. Acta B*, **57**, 121 (2002).
17. Amoruso S. *Appl. Phys. A*, **69**, 323 (1999).
18. Mao X., Russo R.E. *Appl. Phys. A*, **64**, 1 (1997).

19. Antipov A.A., Grasyuk A.Z., Efimovskii S.V., Kurbasov S.V., Losev L.L., Soskov V.I. *Kvantovaya Elektron.*, **25**, 31 (1998) [*Quantum Electron.*, **28**, 29 (1998)].
20. Goncharov V.K. *Inzh.-Fiz. Zh.*, **74**, 87 (2001).
21. Zel'dovich Ya.B., Raizer Yu.P. *Physics of Shock Waves and High-Temperature Hydrodynamic Phenomena* (New York: Academic Press, 1966, 1967) Vols 1 and 2.
22. Lunney J.G., Jordan R. *Appl. Surf. Sci.*, **127 – 129**, 941 (1998).
23. Kas'yanov V.A., Starostin A.N., in *Khimiya Plazmy* (Moscow: Energoatomizdat, 1990) No. 16, p. 67.
24. Beterov I.M., Ishchenko V.N., Kochubei S.A., Kurochkin V.L. *Opt. Commun.*, **54**, 100 (1985).